Electroencephalography and clinical Neurophysiology, 92 (1994) 433–441

EEP 93148

Local estimate of surface Laplacian derivation on a realistically shaped scalp surface and its performance on noisy data

Jian Le *, Vinod Menon and Alan Gevins

EEG Systems Laboratory and SAM Technology, 101 Spear Street, San Francisco, CA 94105 (USA)

(Accepted for publication: 14 March 1994)

Summary A new implementation of the surface Laplacian derivation (SLD) method is described which reconstructs a realistically shaped, local scalp surface geometry using measured electrode positions, generates a local spectral-interpolated potential distribution function, and estimates the surface Laplacian values through a local planar parametric space using a stable numerical method combining Taylor expansions with the least-squares technique. The implementation is modified for efficient repeated SLD operations on a time series. Examples are shown of applications to evoked potential data. The resolving power of the SLD is examined as a function of the spatial signal-to-noise (SNR) ratio. The analysis suggests that the Laplacian is effective when the spatial SNR is greater than 3. It is shown that spatial low-pass filtering with a Gaussian filter can be used to reduce the effect of noise and recover useful signal if the noise is spatially incoherent.

Key words: Evoked potentials; Spatial enhancement; Surface Laplacian derivation; Realistic head shape; Spectral interpolation; Taylor expansion; Spatial filtering

1. Introduction

Neuroelectric signals recorded at the scalp are principally distorted by the effects of the skull and other intervening conductive tissues. This distortion acts as a spatial low-pass filter which causes the potentials at the scalp to appear blurred. In addition, the interpretation of the measured scalp potential distribution is complicated by the unknown contribution of activity at the reference site. Though a true distortion correction method relies on the geometric information about the conducting volumes through which the transmitted scalp signals are distorted, a simple signal enhancement method, called the surface Laplacian derivation (SLD) (Hjorth 1975; Katznelson 1981), can be applied to the blurred scalp data to improve the spatial frequency resolution and to eliminate the common activity at all electrodes. Here SLD denotes the application of the Laplacian operator to a spatial potential distribution function U(x,y,z), confined to a surface S.

There are 2 general approaches to implementing the surface Laplacian algorithm. One approach, which we refer to as a *local* approach, locally estimates the SLD at an electrode using a numerical Laplacian estimator. A typical example of this approach is Hjorth's second order, finite difference scheme (Hjorth 1975) which assumes a planar scalp surface and a rectangular electrode montage to facilitate the second order finite difference calculations. Hjorth's scheme was later improved by Wallin and Stålberg (1980), Hjorth (1980), Katznelson (1981), Nunez (1981) and Thickbroom et al. (1984), whose implementations allow for non-rectangular electrode montages. The resulting "nearest neighbor" SLD, though still based on the planar surface assumption, is approximated by *an average of the directional derivatives from each surrounding electrode to the given electrode*. Greer (1989), Gevins (1989) and Gevins et al. (1990) generalized the nearest neighbor SLD to accommodate non-planar scalp surfaces. For a given electrode, their implementation: (i) finds neighboring electrodes within a chosen search radius, (ii) determines a local optimal plane to fit this set of electrodes (including the given electrode) using the least-squares technique, and (iii) estimates the Laplacian on this local tangent plane using measured potential values at the given electrode and its neighbors. The drawback of this implementation is that it sometimes suffers from a numerical instability problem when the chosen electrodes within a local search radius are too close together. Also, when the interelectrode spacing is larger

* Corresponding author. Tel.: 415-957-1600; Fax: 415-546-7121.

SSDI 0013-4694(94)00096-4

than ~3 cm, the resulting local optimal plane might not be a good approximation to the local scalp surface.

The other approach, which we refer to as *global*, estimates the SLD by first constructing a global interpolation function and then directly applying a Laplacian differentiation operation to the global function. A notable example of this approach is Perrin et al.'s (1987) spherical spline interpolation scheme. In this implementation, a spherical or ellipsoidal surface is used to approximate the scalp surface, and the original measured electrode positions are projected onto the chosen approximation surface. A global interpolation function is generated using the projected positions and the measured potentials at the corresponding original electrodes, and the SLD value is calculated by applying direct differentiation to the resulting interpolation function (Perrin et al. 1987; Nunez 1989; Law and Nunez 1991; Law et al. 1993).

The *global* approach has advantages and drawbacks. The advantage is that it provides a usable surface model when the given scalp electrode montage has relatively few electrodes, say 19, 24. The disadvantages are that (1) it sometimes produces a distorted surface model when the given set of electrodes is concentrated in a small region of scalp surface, or when a dense, say 128-channel, electrode montage is used; (2) it sometimes produces a distorted Laplacian estimate due to its global mathematical interpolation scheme. In this regard, Biggins et al. (1991) and Fein et al. (1991) concluded that "any method of estimating the Laplacian at an electrode site that assigns relatively high weights to data from relatively distant electrodes results in positively biased coherences between electrode sites"; and (3) the direct differentiation performed on the resulting interpolation function is based on the questionable assumption that the higher order derivatives of the interpolation function approximate the higher order derivatives of the original potential distribution function.

The implementation presented here strictly complies with the definition of the surface Laplacian and with the notion that only local information about potentials and about the shape of the scalp surface is needed to estimate the SLD. It improves upon previous efforts in that it first constructs a realistically shaped scalp surface from a given set of 3-D electrode positions, and then, for a chosen electrode, identifies a local scalp surface (which contains the surrounding electrodes) from that surface. It then constructs a local spectral interpolation function utilizing the potentials at the electrodes within the identified local scalp surface to approximate the local potential distribution function. Finally, it estimates the Laplacian value within a planar parametric space associated with the identified 3-D local scalp surface, using a set of potential values generated by the local spectral interpolation function through Taylor expansions and the least-squares technique. Each of the 4 steps is novel, and taken together constitute a new SLD implementation.

The following sections describe the development and the application of the new implementation. Section 2 discusses the theoretical formulations and Section 3 considers various aspects of the implementation. Section 4 presents applications of the method to human evoked potential data, while Section 5 considers the effect of noise and methods to reduce its effect. Future work and some summary comments about the SLD are discussed in Section 6.

2. Theoretical formulations

It is known that any 3-D surface S can be represented in its parametric space $\xi\eta$ such that: $x = f(\xi,\eta)$, $y = g(\xi,\eta)$ and $z = h(\xi,\eta)$. When a given scalp surface is represented in its parametric space, the scalp potential distribution function U(x,y,z) becomes

$$U(x,y,z) = U(f(\xi,\eta), g(\xi,\eta), h(\xi,\eta)) = V(\xi,\eta) \tag{1}$$

and the surface Laplacian operation on U(x,y,z) at a scalp electrode (x_0,y_0,z_0) is thus defined as follows:

$$\nabla\cdot\nabla\ V(\xi,\eta) = \frac{\partial^2 V}{\partial \xi^2} + \frac{\partial^2 V}{\partial \eta^2}, \quad \text{at } \xi_0, \eta_0$$

such that

$$x_0 = f(\xi_0,\eta_0), \quad y_0 = g(\xi_0,\eta_0), \quad z_0 = h(\xi_0,\eta_0).$$

It is evident from this formulation that the surface Laplacian operation is actually a standard Laplacian operation within a parametric space. Therefore, to derive the desired surface Laplacian value at electrode (x_0,y_0,z_0) it is only necessary to obtain a standard Laplacian estimate at point (ξ_0,η_0) within the local parametric space.

For example, when a spherical scalp surface is assumed, the scalp surface can be represented in its parametric space such that

$$x = f(\xi,\eta) = R\cos(\eta)\sin(\xi), \quad y = g(\xi,\eta) = R\sin(\eta)\sin(\xi),$$
$$z = h(\xi,\eta) = R\cos(\xi) \tag{2}$$

Then the surface Laplacian value at electrode (x_0,y_0,z_0) is estimated by applying a standard Laplacian operation to function $V(\xi,\eta)$ at point (ξ_0,η_0), which can be approximated by a second order finite difference scheme around (ξ_0,η_0). The discrete potential values $V(\xi,\eta)$ involved in the finite difference scheme (for this particular kind of scalp surface) are calculated using the relations depicted in Eqs. (1) and (2).

As another example, if a planar scalp surface is assumed, the scalp surface can be represented in its parametric space such that

$$x = f(\xi,\eta) = \xi, \ y = g(\xi,\eta) = \eta, \ z = h(\xi,\eta) = z_0. \tag{3}$$

Then the surface Laplacian value at electrode (x_0,y_0,z_0) is estimated by applying a standard Laplacian operation at point (ξ_0,η_0), which can be approximated by a second order finite difference scheme around (ξ_0,η_0) which is actually point (x_0,y_0) according to Eq. (3). The discrete potential values $V(\xi,\eta)$ involved are actually $U(x,y,z_0)$ since $x=\xi$ and $y=\eta$. Therefore the second order finite difference operation within its parametric space is actually a second order finite difference operation within its original Cartesian coordinates, which happens to be the well-known Hjorth implementation. That means that the Hjorth method is actually a second order finite difference scheme within a local parametric space of a planar scalp surface. This is consistent with the *theory* that the surface Laplacian has to be estimated as a standard Laplacian operation within its parametric space.

3. Implementation

In this section, we discuss a method which estimates the surface Laplacian of a potential distribution function U(x,y,z) defined at surface S through a standard Laplacian operation within its local parametric space. The implementation discussed here assumes that discrete potential values of U(x,y,z) are given only at electrodes (x_i,y_i,z_i) ($i=1, 2, \ldots, N$) on a scalp surface S. For notational simplicity, we shall denote $U(x_i,y_i,z_i)$ by U_i hereafter.

3.1. Reconstruction of global scalp surface S and local scalp surfaces within S

Surface S is reconstructed from the given set of electrodes (x_i,y_i,z_i) ($i=1, 2, \ldots, N$) on S through a step-wise triangularization procedure designed primarily for convex surfaces with no folding. In the first step, the 2 closest neighboring electrodes of any selected electrode are found which determine the first triangle in the mesh and the current mesh boundary. In the next step, the closest electrode outside the mesh boundary is determined, a new triangle is defined and the mesh boundary is revised. This is repeated until all electrodes from the given set have been incorporated into this triangular mesh. To ensure a convex mesh boundary, a triangle using 3 consecutive electrodes on the current mesh boundary is added into the mesh after each step, if necessary. At the end, all adjacent triangles are checked to see if an obtuse angle might be reduced by substituting 2 alternative triangles.

The resulting triangular mesh serves as an organizational framework for the electrodes within the montage. For every electrode (x_0,y_0,z_0) on S, a sublist of polygons (triangles), which have electrode (x_0,y_0,z_0) as one of their vertices, is extracted from the global list. If the resulting polygons in the sublist form a complete circle around (x_0,y_0,z_0), this electrode is classified as an *internal* point. The corresponding sublist of polygons is defined as "the local polygon surface associated with (x_0,y_0,z_0)" and is denoted by S_0. Otherwise this electrode is classified as an *edge* (peripheral) point whose surface Laplacian value is not defined because the information of local potential distribution around this point is not complete.

The local polygon surface associated with (x_0,y_0,z_0) plays an important role in the implementation. It defines a local surface, helps to construct the local parametric space and helps to generate a local spectral potential interpolation function. In the appendix, one method is presented which constructs the local parametric representation functions $f(\xi,\eta)$, $g(\xi\eta)$ and $h(\xi,\eta)$ using various features associated with S_0.

3.2. Construction of local interpolation function within the local surface

When the standard Laplacian value is estimated at point (ξ_0,η_0) using a numerical scheme, it usually involves potentials at its neighboring points (ξ_1,η_1), which are calculated using the formula in Eq. (1). Since the mapped point $(f(\xi_1,\eta_1), g(\xi_1,\eta_1), h(\xi_1,\eta_1))$ is not necessarily a given electrode position where the potential value is known, an interpolated potential distribution function within S_0 is needed to facilitate the standard Laplacian operation within its parametric space. For convenience, we denote the position of the given electrode by (x_0,y_0,z_0), the positions of its n surrounding electrodes in S_0 by (x_k,y_k,z_k), and the corresponding measured potentials at (x_k,y_k,z_k) by U_k, $k=0, \ldots, n$.

A common choice of the interpolation scheme is the piecewise linear interpolation function on S_0, which is composed of the linear interpolation function over each polygon included in the local polygon surface S_0. However a preferred interpolation scheme is the local spectral function P(x,y,z) on S_0, which is active near the area of interest and dormant outside this region. One of the functions in use for S_0 with n surrounding electrodes (x_k,y_k,z_k), for example, has the following form:

$$P(x,y,z)=\sum_{k=0}^{n}\left[a_k/\left((x-x_k)^2+(y-y_k)^2+(z-z_k)^2+w^2\right)^{1/2}\right]+a_{n+1}. \tag{4}$$

The coefficients a_k ($k=0, 1, \ldots, n+1$) are determined by solving a set of simultaneous linear equations which force the interpolated values at the electrode positions to be equal to the measured potentials U_k, $k=0, 1, \ldots, n$, and which satisfies the following:

$$\sum_{k=0}^{n} U_k=(n+1)\sum_{j=0}^{n+1} a_j.$$

Function P(x,y,z) defined in Eq. (4) is a local spectral function as it is a linear combination of reciprocals of the distance functions. A non-zero constant w assures that function P(x,y,z) is infinitely differentiable. We choose w to be the average inter-electrode distance of all electrodes in the given montage measured over the scalp surface.

3.3. Standard Laplacian operator

To derive the desired quantities $\partial^2 V/\partial\xi^2$ and $\partial^2 V/\partial\eta^2$ at (ξ_0,η_0), either Hjorth's scheme or the "nearest neighbor" implementation could be used here since the parametric space (ξ,η) is a planar surface. However to enhance the numerical accuracy and stability, a scheme similar to the "averaged directional derivatives from each surrounding point to the given point" is adopted here through a 6-term Taylor expansion of 12 equally spaced surrounding points (ξ_l,η_l), each at a radial distance ϵ from (ξ_0,η_0) such that:

$$\begin{aligned} &V(\xi_l,\eta_l)-V(\xi_0,\eta_0)\\ &\approx \frac{\partial V(\xi_0,\eta_0)}{\partial\xi}(\xi_l-\xi_0)+\frac{\partial V(\xi_0,\eta_0)}{\partial\eta}(\eta_l-\eta_0)\\ &+\frac{\partial^2 V(\xi_0,\eta_0)}{\partial\xi^2}(\xi_l-\xi_0)\times(\xi_l-\xi_0)/2\\ &+\frac{\partial^2 V(\xi_0,\eta_0)}{\partial\eta^2}(\eta_l-\eta_0)\times(\eta_l-\eta_0)/2\\ &+\frac{\partial^2 V(\xi_0,\eta_0)}{\partial\xi\partial\eta}(\xi_l-\xi_0)\times(\eta_l-\eta_0). \end{aligned} \tag{5}$$

When $V(\xi_l,\eta_l)$ $(l=1,\ \ldots,\ 12)$ and $V(\xi_0,\eta_0)$ are available, the desired quantities $\partial^2 V/\partial\xi^2$ and $\partial^2 V/\partial\eta^2$ at (ξ_0,η_0) are uniquely determined using a least-squares technique [1]. The ϵ is chosen to be one tenth of the averaged distance between the given electrode and the surrounding electrodes.

3.4. Surface Laplacian derivation operation

In practice, for a given point (x_0,y_0,z_0) and its local surface S_0, its parametric representation $(x=f(\xi,\eta),\ y=g(\xi,\eta),\ z=h(\xi,\eta))$ is sought first. Then the points (ξ_0,η_0) and (ξ_l,η_l) are determined within the resulting parametric space, and the set of equations in Eq. (5) is set up. Third, the local spectral potential distribution function P(x,y,z) is constructed. Fourth, the function values $V(\xi_l,\eta_l)$ $(l=1,\ 2,\ \ldots,\ 12)$ are calculated by the local interpolation function $P(f(\xi_l,\eta_l),\ g(\xi_l,\eta_l),\ h(\xi_l,\eta_l))$, and the function value $V(\xi_0,\eta_0)$ equals $P(x_0,y_0,z_0)$, which in turn is the measured potential value at the given electrode. Finally, the set of equations in Eq. (5) is solved by a least-squares method.

The described implementation has also been modified for Laplacian operations on a series of time points. It is based on the observation that for any given *internal* electrode, its local polygon surface, the structure of the local spectral interpolation function, and the numerical Laplacian operator for this given electrode are unchanged from one time point to another. Therefore in a modified version of the above implementation, a time invariant Laplacian *weight vector* associated with each *internal* electrode is explicitly constructed, which yields the desired surface Laplacian estimate at each *internal* electrode through a dot product operation of its *surface Laplacian weight vector* and a potential vector consisting of the measured EEG data on S_0 at a given time point, and a given trial. In a numerical experiment in which the original surface Laplacian and the modified surface Laplacian were applied to a time series of 300 time points, the modified implementation was found to be 60 times faster.

4. Surface Laplacians of evoked potential data

In this section, we apply the new SLD method to sensory evoked potentials. The linked-mastoid scalp potential maps and their corresponding surface Laplacian maps are displayed for 1 subject receiving 14.92 Hz electrical finger stimulation. The colored surface maps were produced when the potential values or the corresponding surface Laplacian values were aligned with a scalp surface geometry obtained from the subject's magnetic resonance images (MRIs) (Gevins et al. 1994).

For a normal subject (coded MS3), steady-state EPs were elicited by a mild 14.92 Hz electrical pulse of 0.2 msec width applied to the left middle and right index fingers [2]. Three 100 sec blocks of EEG were recorded from 122 scalp channels, and digitized at 128 Hz with a bandpass of 0.5–50 Hz. Artifact-free epochs of 0.53125 sec were averaged for each channel, and a noise reduction method was applied to the averaged time series.

[1] In Eq. (5), the Taylor expansion was truncated after the third term to constitute a numerical Laplacian estimator. It could have been truncated at a later term at the cost of introducing higher order partial derivatives. In application to EEG studies, we have found that a 6-term approximation is sufficient. Adequate spacing between neighboring points assures numerical stability in solving the resulting least-squares problem represented by Eq. (5) for $l=1,\ 2,\ \ldots,\ 12$. Also the choice of this Laplacian montage within the parametric space guarantees that the corresponding Laplacian operator has a symmetric weight distribution around the given point, which reflects an important embedded property of the surface Laplacian operation. When surface S is planar, the proposed implementation becomes a modified Hjorth method in which 12 equally spaced neighboring points are used.

[2] The stimulation protocol included occasional omissions of one of the stimuli. The subject had to count these missing stimuli and report the tally at the end of each 100 sec block.

The noise reduction method was carried out as follows. A Hanning taper was applied to each time series, the Discrete Fourier Transform (DFT) was computed, and the real and imaginary spectral amplitude values were extracted for all components (within the recording bandpass) harmonically related to the stimulation frequency. Non-harmonic frequency bins were zeroed, and the inverse DFT was applied to each block to reconstruct the averaged time series, thus effectively rejecting the noise that was not harmonically related to the steady-state signal (Nakamura et al. 1989).

The reconstructed signals at 122 electrodes were averaged over 3 blocks, and SLDs were computed at the latency at which the maximal spatial energy occurred. To demonstrate the increase in spatial detail by utilizing more electrodes and by applying surface Laplacian operations, the potential data were spatially downsampled to montages with 57, 31 or 18 electrodes (Fig. 1a), and the corresponding SLDs were computed (Fig. 1b). Since the site of maximal response occurred over an area not included in the 18-channel montage, the 18-channel potential map shows a maximum response which is too anterior for the left middle finger stimulation, a typical undersampling problem. This problem is gradually corrected as more spatial information is obtained by increasing the number of channels. Fig. 1b displays the SLDs corresponding to Fig. 1a. It is apparent that the SLD sharpens the maps, especially around the maxima and minima of potential. This is expected since the Laplacian operation measures the second spatial derivative of potential. The importance of utilizing more electrodes is also evident in the posterior shift and increased definition of the maxima with an increasing number of recording sites.

5. Practical considerations: effect of noise

The Laplacian is highly sensitive to noise because it is a process which amplifies high spatial frequencies. The precise nature of this amplification process can be derived as follows. If the potential distribution is expressed as $\Phi(r) = -\int \Psi(k) e^{i2\pi kr} dk$ its Laplacian will be

$$\nabla^2\Phi(r) = 4\pi^2 \int k^2 \Psi(k)\, e^{i2\pi kr}\, dk \qquad (6)$$

where r is the radius in polar coordinates and k is the spatial frequency in cycles/cm. The ratio of the integrand in Eq. (6) over the integrand in the potential expression reveals that the transfer function of the Laplacian is $4\pi^2 k^2$. This quadratic scaling factor explains the noise amplification phenomenon commonly seen in applications of the Laplacian. However, if a spatial low-pass filter is applied to noisy data before the Laplacian is computed, this amplification of noise can be mitigated. A typical low-pass filter is the convolution with the Gaussian: $(1/2\pi\sigma^2)e^{-r^2/2\sigma}$, where r is the radius in polar coordinates and σ is the standard deviation of the Gaussian. It is straightforward to show that the combined transformation, Gaussian and Laplacian, has the following transfer function:

$$\Sigma(k) = 4\pi^2 k^2\, e^{-2\pi^2 k^2 \sigma^2}$$

whose profile is displayed in Fig. 2 with σ set at 1.94. The transfer function shows that the combined operation acts as a bandpass filter tuned to spatial frequencies in the neighborhood of $k = 1/\sqrt{2}\pi\sigma$.

The effect of noise and spatial low-pass filtering was first investigated with simulated data. Noise-free scalp potentials were generated using a 3-concentric sphere model which had radii of 9 cm, 8.5 cm and 8 cm respectively. Two radial point dipoles were placed at a depth of 0.5 cm under the cortical surface. In order to examine the resolving power of the SLD, the distance between the sources was increased along an arc subtending 20°, 40°, 60°, 90°, 120°. This corresponds to distances of 2.61, 5.23, 7.85, 11.78, 15.70 cm at the cortical surface and 3.14, 6.28, 9.42, 14.14, 18.85 cm at the scalp surface. The noise-free scalp data were calculated at 91 electrodes on the outer spherical surface. Gaussian noise (zero mean and unit standard deviation) was properly scaled and added to the noise-free scalp data to generate scalp data with spatial signal-to-noise ratio (SNR) ranging from 0.25, 0.5, 1.0 1.5, 2.0, 3.0, 4.0, 6.0, 10.0 to infinity. SNR was defined as RMS signal to RMS noise ratio.

SLDs were derived for each noisy data set corresponding to different source configurations. Then the relative errors of SLDs were computed when the noisy SLDs were compared to the noise-free SLDs and normalized by the same noise-free SLDs. Fig. 3 displays (solid line) the relative errors of the SLD as a function of the SNR for the source configuration in which 2 radial point dipoles are 40° apart. The effect of using a low-pass spatial (Gaussian) filter for the same set of data is shown as dashed line in Fig. 3. A σ value of 1.94 was used for the Gaussian filter; this corresponds to the 26 dB down point of the Gaussian for an inter-electrode distance of 2.5 cm. The results show that spatial smoothing is effective for SNRs ranging from ~ 3 to ~ 6. For data whose spatial SNR is less than 3, noisy spurious isolated peaks were found for all chosen source configurations.

The effect of noise and spatial filtering was then investigated with somatosensory evoked potentials (EPs). The SLD, with and without spatial filtering, was computed from 59-channel somatosensory EPs elicited by a mild 2.22 Hz electrical pulse of 0.2 msec width applied to the right index finger of a normal subject (coded MS14). Averages were made using 100, 300, 1000 and 1800 trials and the N30/P30 components

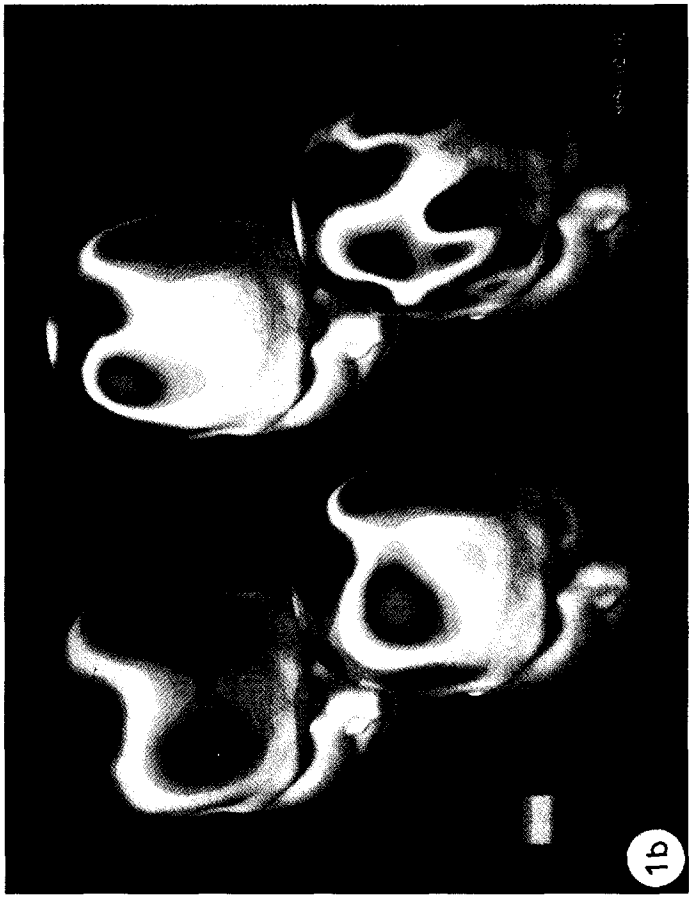

1a

1b

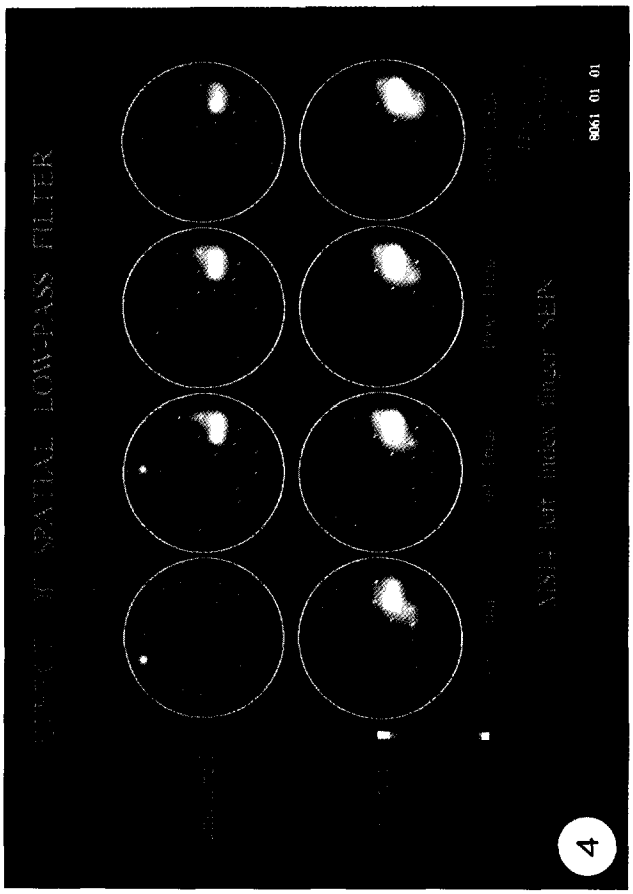

4

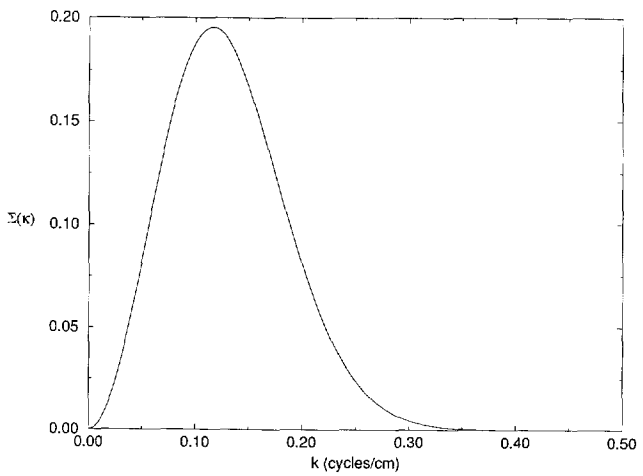

Fig. 2. Transfer function of the combined SLD and Gaussian low-pass spatial filter. The profile shows that the combined operation acts as a spatial bandpass filter tuned to spatial frequencies in the neighborhood of $k = 1/(\sqrt{2}\pi\sigma)$ for σ set at 1.94.

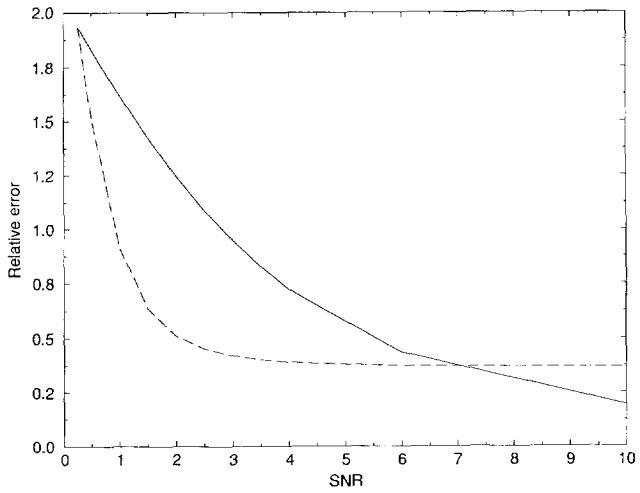

Fig. 3. Relative error of SLD as a function of the spatial signal-to-noise ratio (SNR) of data generated by a 2-point dipole source model with additive Gaussian noise (zero mean and unit standard deviation). Two radial dipole sources are 0.5 cm under the cortical surface and 40° apart. The solid line represents the relative errors obtained without using spatial filtering operations whereas the dashed line represents the relative errors derived with Gaussian spatial low-pass filtering ($\sigma = 1.94$). A sharp reduction in relative errors of the SLD is observed for data whose spatial SNRs range between ~3 and ~6.

(whose underlying source is well modeled by a tangential dipole localized to area 3b) were extracted from the averages. Spatial filtering removes the spurious peaks from the 300 trial average for which the SNR is about 3 [3], whereas a spurious frontal peak remains for averaged data using 100 trials for which SNR < 1 (Fig. 4).

In summary, the SLD produces spurious results when the spatial SNR is less than ~3. A spatial low-pass Gaussian filter can be used to reduce the amplification of noise. The filter is effective if the SNR of the signal lies between ~3 and ~6. The cost of this noise reduction is, of course, reduced spatial resolution. The SLDs displayed in Fig. 1b were derived without spatial prefiltering because the SNRs of the data were high (> 10).

Before we leave this section, we would also like to point out that the uncertainty in the measurement of electrode positions poises another source of error in the estimation of the surface Laplacian. Though rigorous error analysis shows that the effects of this uncertainty can be large, we have experienced no significant change of surface Laplacian patterns when the given electrode montage was perturbed. The perturbation was done by projecting the original electrode montage to another subject's actual scalp head shape derived from the latter's magnetic resonance images.

6. Conclusion

The surface Laplacian derivation is a useful tool with which to qualitatively reduce the blurring effect of volume conduction on scalp-recorded EEGs and to eliminate the dependence on the reference electrode. A realistically shaped surface model has been used in the described implementation to preserve an accurate

[3] The spatial SNRs for the EPs using 100, 300 and 1000 trials were estimated as RMS of EP with 1800 trials divided by RMS of the residual of the EP with respect to 1800 trials. This necessarily results in a conservative estimate of the SNR.

Fig. 1. a: effect of an increasing number of electrodes on evoked potential topography. The response to repetitive electrical stimulation of the left middle and right index fingers was mapped onto a scalp surface reconstructed from the subject's horizontal MR images. The maps, made with 18, 31, 57 and 122 channels referenced to digitally linked mastoids, show a progressive increase in spatial detail. Since the site of maximal response occurred over an area not included in the 18-channel montage, the 18-channel potential map shows a maximum response which is too anterior, a problem which is gradually corrected as more channels are used. The white dots represent the electrode positions measured on the scalp. b: surface Laplacian derivation computed from the potential maps of a. The blurring evident on the potential maps has been largely reduced. As a result, the maxima and minima are more prominent. The posterior shift and increased definition of the maxima with an increasing number of recording sites is evident.

Fig. 4. SLD maps for the N30/P30 somatosensory EP component generated using 100, 300, 1000, and 1800 trials. SLD maps without spatial low-pass filtering (upper row) have a spurious frontal maximum when 300 or 100 trials are used. Applying spatial low-pass filtering to the data (lower row) removes the spurious maximum in the 300-trial average. The spurious maximum remains in the 100-trial average in which the SNR is less than 1.

representation of the scalp potential distribution. A numerically stable surface Laplacian estimator has been designed and developed which utilizes a local planar parametric space, a local spectral interpolation function, Taylor expansions and the least-squares technique. Like other implementations, ours does not attempt to estimate the SLD at peripheral electrodes of the recording montage, simply because the local potential information around a peripheral electrode is not completely defined. Also, as with all other SLD implementations, the location of an extremum in the SLD map may not overlv the location of the potential extrema because the SLD is the second spatial derivative of potential and is maximal where the gradient of the field is changing most rapidly.

As a signal processing method, the quality of the SLD solely depends upon the quality of the input data $\{U(x_i,y_i,z_i),\ i = 1,\ \ldots,\ N\}$. Any perturbation of the measured electrode positions (x_i,y_i,z_i) from the actual positions or of the measured potential values U_i at these positions will severely perturb the SLD estimates. This is an inherent problem of the SLD resulting from the fact that a spatial distribution function is differentiated twice in its parametric space. In general, the SLD is noisy when the spatial signal-to-noise ratio is less than about 3. A spatial low-pass filter such as a Gaussian can be used in conjunction with the SLD to reduce the effect of noise. This assumes that noise is spatially incoherent and has high spatial frequency. The presence of correlated noise, as well as overlapping noise and signal spectra, are likely to degrade the performance further. The issue of correlated noise is an important one. However, there is a priori no one good way to generate correlated noise since, in principle, noise statistics can vary from completely overlapped with the signal to completely uncorrelated. Analysis of correlated noise on the basis of EEG statistics is beyond the scope of this paper. The SLD implementation described here can be further improved by improving the proximity of the triangularized polygon surface to the original scalp surface, by finding a better spectral interpolation function, and by obtaining a more accurate parametric representation of the local scalp surface. However, it is perhaps of more basic concern to make improvements in collecting data with a high SNR and in obtaining accurate measurements of the electrode positions.

Finally, we would like to point out that the SLD does not use information about a subject's internal tissue geometries and their conducting properties (e.g., the thicknesses and conductivities of scalp, skull and diploe layers). The SLD uniformly sharpens a potential map on a surface and produces a spatial pattern similar to that which would be recorded at the bottom of a uniform and homogeneous slab attached to the given surface. Since the scalp, CSF and especially the skull are not homogeneous materials, the SLD can not be expected to accurately estimate the pattern at the cortical surface. If this is desired, a distortion correction method which explicitly models the conducting properties of scalp and skull is required (Gevins et al. 1991, 1994; Le and Gevins 1993).

This research was supported by the National Institute of Neurological Diseases and Strokes, the National Institute of Mental Health, the Air Force Office of Scientific Research, the National Science Foundation, and the Office of Naval Research.

Technical contributions and assistance with the research presented here were also made by our colleagues at EEG Systems Laboratory and SAM Technology including Jim Alexander, Paul Brickett, Brian Cutillo, John Desmond, Frank Luo, Nancy Martin, Judy McLaughlin, Bryan Reutter and Mike Ward, and by Prof. Walter Freeman at UC Berkeley.

Appendix

For an arbitrary surface S, the global expressions of its parametric representations $f(\xi,\eta)$, $g(\xi,\eta)$ and $h(\xi,\eta)$ defined in Eq. (1) are, in general, not available. However, a local expression of a local parametric surface can be constructed. For estimating the surface Laplacians, only a local parametric surface is needed.

As discussed in Section 2, features of a local polygon surface S_0 will be used to help construct the local parametric space. It is known that the resulting local polygon surface itself is an approximation to the exact local scalp surface. Therefore a parametric surface which is equally influenced by the available local polygon surface and the exact local scalp surface will be desirable. We find that the tangent plane attached to S at point (x_0,y_0,z_0) is a good choice, simply because it coincides with the local polygon surface and the exact local scalp surface at point (x_0,y_0,z_0), and because it usually approximates the exact local scalp surface better than the corresponding local polygon surface does in the close neighborhood of (x_0,y_0,z_0). In the following, we will describe how to construct this local tangent plane at point (x_0,y_0,z_0) based on the information carried along by the associated local polygon surface S_0.

Assume that the normal direction vector of surface S at point (x_0,y_0,z_0) is (p_x,p_y,p_z). Then the following process will produce the desired parametric representations.

Step 1. Move the origin to (x_0,y_0,z_0). The corresponding transformation is:

$$\begin{bmatrix} x' \\ y' \\ z' \end{bmatrix} = \begin{bmatrix} x-x_0 \\ y-y_0 \\ z-z_0 \end{bmatrix} \tag{A.1}$$

Step 2. Rotate the positive z′ axis defined in Eq. (A.1) into the normal direction $(p_x,p_y,p_z)^t$ which is

unchanged under step 1. The rotation is carried out by 2 planar rotations with the first one rotating an angle of ϕ_0 about the z′ axis and the second one rotating an angle of θ_0 about the y′ axis, such that

$$\begin{bmatrix} x'' \\ y'' \\ z'' \end{bmatrix} = T \begin{bmatrix} x' \\ y' \\ z' \end{bmatrix} \tag{A.2}$$

where

$$T = \begin{bmatrix} \cos\theta_0 & & -\sin\theta_0 \\ & 1 & \\ \sin\theta_0 & & \cos\theta_0 \end{bmatrix} \begin{bmatrix} \cos\phi_0 & \sin\phi_0 & \\ -\sin\phi_0 & \cos\phi_0 & \\ & & 1 \end{bmatrix},$$

$$\cos\phi_0 = p_x / \left(p_x^2 + p_y^2\right)^{1/2}, \qquad \sin\phi_0 = p_y / \left(p_x^2 + p_y^2\right)^{1/2},$$

$$\cos\phi_0 = p_z / \left(p_x^2 + p_y^2 + p_z^2\right)^{1/2},$$

$$\sin\theta_0 = \left(p_x^2 + p_y^2\right)^{1/2} / \left(p_x^2 + p_y^2 + p_z^2\right)^{1/2}.$$

The resulting x″y″ space defines the tangent plane at (x_0,y_0,z_0). Setting $x'' = \xi$, $y'' = \eta$, $z'' \equiv 0$, and combining Eq. (A.1) with Eq. (A.2) we get

$$\begin{bmatrix} \xi \\ \eta \\ 0 \end{bmatrix} = T \begin{bmatrix} x - x_0 \\ y - y_0 \\ z - z_0 \end{bmatrix}. \tag{A.3}$$

Premultiplying T^{-1} to both sides of the above equation and using the fact that $T^{-1} = T^t$ since T is orthogonal, Eq. (A.3) can be rearranged into:

$$\begin{bmatrix} x \\ y \\ z \end{bmatrix} = T^t \begin{bmatrix} \xi \\ \eta \\ 0 \end{bmatrix} + \begin{bmatrix} x_0 \\ y_0 \\ z_0 \end{bmatrix} = \begin{bmatrix} f(\xi,\eta) \\ g(\xi,\eta) \\ h(\xi,\eta) \end{bmatrix}. \tag{A.4}$$

In our programmed implementation, the normal direction vector (p_x,p_y,p_z) of surface S at point (x_0,y_0,z_0) is estimated through the weighted average of the normal direction vectors of n polygons included in the local polygon surface associated with electrode (x_0,y_0,z_0),

$$(p_x,p_y,p_z)^t = \frac{\sum_1^n (\alpha_j \mathbf{I}_j)}{\sum_1^n \alpha_j}. \tag{A.5}$$

Here α_j is the jth weight and $\mathbf{I}_j$ is the normal direction vector of jth polygon in the list. We choose weight α_j to be the angle of the jth polygon whose vertex is (x_0,y_0,z_0). This weighting scheme is reasonable because when the polygons in the list lie in one plane, the resulting $(p_x,p_y,p_z)^t$ should be the normal direction vector of the same plane. This expectation is satisfied by Eq. (A.5) because, when that happens, the normal direction vector of each polygon involved will be identical and is the same as the normal direction vector $\mathbf{I}_p$ of the plane. When the $\mathbf{I}_j$ are identical, it can be factored out of the numerator of Eq. (A.5) since it is a common factor. The sums of the weights which appeared in the numerator and the denominator are canceled with each other. That leaves $(p_x,p_y,p_z)^t$ equal to $\mathbf{I}_j$ which equals $\mathbf{I}_p$ in this particular case.

References

Biggins, C., Fein, G., Raz, J. and Amir, A. Artifactually high coherences result from using spherical spline computation of scalp current density. Electroenceph. clin. Neurophysiol., 1991, 79: 413–419.

Fein, G., Raz, J. and Turetsky, B. Brain electrical activity: the promise of new technologies. In: S. Zakhari and E. Witt (Eds.), Imaging in Alcohol Research. Proc. of a Workshop on Imaging in Alcohol Research, Wild Dunes, SC, 9–11 May, 1991: 49–78.

Gevins, A.S. Dynamic functional topography of cognitive tasks. Brain Topogr., 1989, 2: 37–56.

Gevins, A.S., Brickett, P., Costales, B., Le, J. and Reutter, B. Beyond topographic mapping: towards functional-anatomical imaging with 124-channel EEGs and 3-D MRIs. Brain Topogr., 1990, 3: 53–64.

Gevins, A.S., Le, J., Brickett, P., Reutter, B. and Desmond, J. Seeing through the skull: advanced EEGs use MIRs to accurately measure cortical activity from the scalp. Brain Topogr., 1991, 4: 125–131.

Gevins, A.S., Le, J., Martin, N., Brickett, P., Desmond, J. and Reutter, B. High resolution EEG: 124-channel recording, spatial deblurring and MRI integration methods. Electroenceph. clin. Neurophysiol., 1994, 90: 337–358.

Greer, D. An Algorithm for Reconstructing the Surface of the Central Nervous System in Vivo. Ph.D. Dissertation, Dept. of EECS, UC Berkeley, Berkeley, CA, 1989.

Hjorth, B. An on line transformation of EEG scalp potentials into orthogonal source derivations. Electroenceph. clin. Neurophysiol., 1975, 39: 526–530.

Hjorth, B. Source derivation simplifies topographical EEG interpretation. Am. J. EEG Technol., 1980, 20: 121–132.

Katznelson, R. EEG recording, electrode placement and aspects of generator localization. In: P. Nunez (Ed.), Electric Fields of the Brain: the Neurophysics of EEG. Oxford University Press, New York, 1981.

Law, S. and Nunez, P. Quantitative representation of the upper surface of the human head. Brain Topogr., 1991, 3: 365–371.

Law, S., Nunez, P. and Wijesinghe, R. High-resolution EEG using spline generated surface Laplacians on spherical and ellipsoidal surfaces. IEEE Trans. Biomed. Eng., 1993, 40: 145–153.

Le, J. and Gevins, A.S. Method to reduce blur distortion from EEGs using a realistic head model. IEEE Trans. Biomed. Eng., 1993, 40: 517–528.

Nakamura, M., Nishida, S. and Shibasaki, H. Spectral properties of signal averaging and a novel technique for improving the signal-to-noise ratio. J. Biomed. Eng., 1989, 11: 72–78.

Nunez, P. (Ed.). Electric Fields of the Brain: the Neurophysics of EEG. Oxford University Press, New York, 1981.

Nunez, P. Estimation of large scale neocortical source activity with EEG surface Laplacians. Brain Topogr., 1989, 2: 141–154.

Perrin, F., Bertrand, O. and Pernier, J. Scalp current density mapping: value and estimation from potential data. IEEE Trans. Biomed. Eng., 1987, 34: 283–288.

Thickbroom, G., Mastaglia, F., Carroll, W. and Davies, H. Source derivation: application to topographic mapping of visual evoked potentials. Electroenceph. clin. Neurophysiol., 1984, 59: 279–285.

Wallin, G. and Stålberg, E. Source derivation in clinical routine EEG. Electroenceph. clin. Neurophysiol., 1980, 50: 282–292.